

Forward-Viewing CMUT Arrays for Medical Imaging

Utkan Demirci, *Student Member, IEEE*, Arif S. Ergun, *Associate Member, IEEE*,
 Ömer Oralkan, *Student Member, IEEE*, Mustafa Karaman, *Member, IEEE*,
 and Butrus T. Khuri-Yakub, *Fellow, IEEE*

Abstract—This paper reports the design and testing of forward-viewing annular arrays fabricated using capacitive micromachined ultrasonic transducer (CMUT) technology. Recent research studies have shown that CMUTs have broad frequency bandwidth and high-transduction efficiency. One- and two-dimensional CMUT arrays of various sizes already have been fabricated, and their viability for medical imaging applications has been demonstrated. We fabricated 64-element, forward-viewing annular arrays using the standard CMUT fabrication process and carried out experiments to measure the operating frequency, bandwidth, and transmit/receive efficiency of the array elements. The annular array elements, designed for imaging applications in the 20 MHz range, had a resonance frequency of 13.5 MHz in air. The immersion pulse-echo data collected from a plane reflector showed that the devices operate in the 5–26 MHz range with a fractional bandwidth of 135%. The output pressure at the surface of the transducer was measured to be 24 kPa/V. These values translate into a dynamic range of 131.5 dB for 1-V excitation in 1-Hz bandwidth with a commercial low noise receiving circuitry. The designed, forward-viewing annular CMUT array is suitable for mounting on the front surface of a cylindrical catheter probe and can provide Doppler information for measurement of blood flow and guiding information for navigation through blood vessels in intravascular ultrasound imaging.

I. INTRODUCTION

CMUTs have emerged in the last decade as a complement and alternative to piezoelectric transducers both in air and immersion applications [1]–[4]. The CMUTs are made of a plurality of thin membranes, and they exhibit relatively low mechanical impedance levels with respect to the surrounding medium. This translates into better acoustic match in air applications and wider frequency bandwidth in immersion applications [5], [6]. In addition, CMUTs are fabricated using standard micromachining processes that provide all the advantages of the integrated circuit technology, such as ease of fabrication, batch production, and repeatability.

In ultrasound imaging systems, wide temporal bandwidth affects the overall imaging performance, such as producing fine axial resolution and allowing different imaging

modalities. This makes CMUTs a good candidate for imaging applications. Recently, we have fabricated fully functional one-dimensional (1-D) CMUT arrays with an element count of 128 and evaluated their performance with pulse-echo imaging experiments [7]. More recently, we also fabricated and tested 2-D CMUT arrays and reported the results in [8], [9]. These studies all have demonstrated that CMUT technology is capable of fabricating arrays with high yield and good performance for imaging applications.

Invasive imaging is becoming a popular branch of medical ultrasound. Guiding ultrasonic arrays through blood vessels or inside the cavities of the human body has many potential applications, such as intravascular imaging, blood flow measurements, and image-guided surgery [10]–[14]. However, the fabrication of ultrasonic arrays suitable for such applications presents a couple of challenges to which micromachining finds easy and elegant solutions. One of the important challenges is the miniaturization of the array elements. The element size of a forward-viewing annular array is limited both in the angular and radial directions to avoid grating lobes in volumetric scans and to provide a large hollow at the center for the guiding wire so that the array can be guided into narrow cavities and vessels. The size and the shape of CMUT array elements are defined with photolithographic techniques; therefore, they can be designed and fabricated ideally in any size and shape. Miniaturization of the array elements brings challenges to the electronics design in relation to the size of each array element. Small sized elements suffer from low signal-to-noise ratio (SNR) on the overall response, and any parasitic capacitance (such as wiring and interconnection capacitances) in the system decreases the output SNR further [15]. Under these circumstances, it is important to bring the receiving electronics as close to the array as possible and to minimize the capacitance of the interconnections. Recently, an efficient method of integrating electrical through wafer interconnects with CMUTs has been demonstrated [16]. With this technology, it is possible to bring the electrical connection of each CMUT element to the back side of the silicon wafer with a parasitic capacitance of 0.05 pF, for connection to the receiving electronics.

This paper reports the design, fabrication, and testing of 64-element, forward-viewing CMUT annular arrays. Section II outlines the standard CMUT technology followed by a detailed description of annular array design and fabrication. The characterization of the array elements to

Manuscript received April 2, 2003; accepted March 2, 2004.

U. Demirci, A. S. Ergun, Ö. Oralkan, and B. T. Khuri-Yakub are with E. L. Ginzton Laboratory, Stanford University, Stanford, CA 94305-4088 (e-mail: utkan@stanford.edu).

M. Karaman is with the Department of Electronics Engineering, Isik University, Istanbul, Turkey.

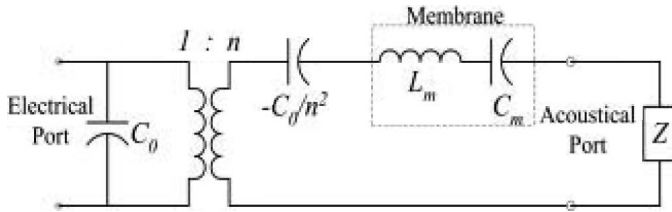


Fig. 1. Equivalent circuit of an electromechanical transducer.

evaluate their performance is presented in Section III. The results are discussed in Section IV.

II. DESIGN AND FABRICATION OF ANNULAR CMUT ARRAYS

CMUTs are made of thin membranes that are essentially parallel plate capacitors with a vacuum gap between the plates. The silicon wafer on which the transducers are fabricated make up one of the plates of the capacitor. The other plate of the capacitor is the metal electrode on top of the membrane. The CMUTs are used as both ultrasonic transmitters and receivers. In transmit mode, the electrostatic attraction force is used to put the membranes into vibration by applying an alternating current (AC) voltage. However, because electrostatic force is unipolar (always attractive), a direct current (DC) voltage is required for operation. In receive mode, the membrane vibrations caused by an incident ultrasound wave are detected using a capacitive detection, which also requires a DC voltage. A detailed description of CMUT operation can be found in [5], [17].

A. Mechanical Impedance and Bandwidth

The analysis of CMUT transducers involves the use of the electrical equivalent circuit modeling introduced by Mason for electro-acoustic devices [18]. In the equivalent circuit shown in Fig. 1, the capacitor on the electrical side is simply the device capacitance of the CMUT element. On the acoustical side, the inductor, L_m , and the capacitor, C_m , represent the complex mechanical impedance of the CMUT because it is a resonant structure. The load, Z , is the acoustical impedance of the surrounding medium, and the negative capacitance on the mechanical side represents the spring softening effect [17]. The transformer represents the electro-mechanical conversion between the electrical and the acoustical port.

Using the electrical circuit analogy, one can see that the bandwidth, or equivalently the Q-factor of this resonant structure, is determined by the acoustical impedance of the medium, assuming that the bandwidth is not limited by the electronics. In immersion applications, the resonant circuit is overdamped with the large acoustical impedance of the medium resulting in a wideband frequency response. Fig. 2 is a plot of the imaginary part of the complex mechanical impedance per area of a small ($80 \mu\text{m}$ by $560 \mu\text{m}$)

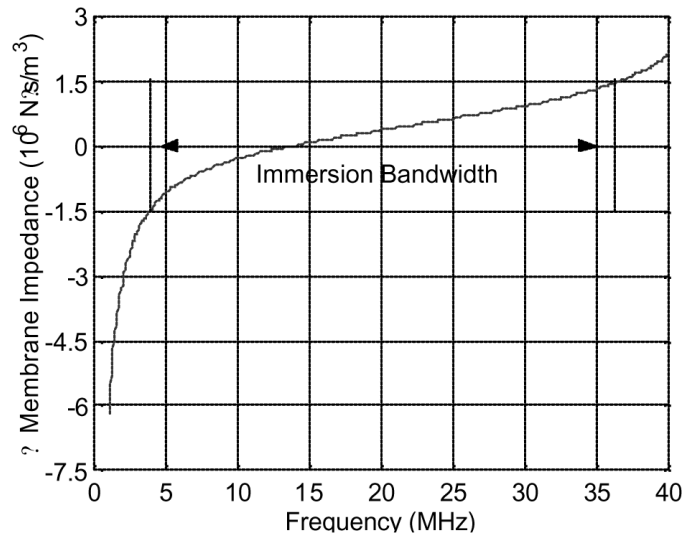


Fig. 2. The mechanical impedance per area of a circular CMUT element designed for operation in the 5–35 MHz range in immersion.

CMUT element. By comparing the mechanical impedance of the CMUT element to the acoustical impedance of water ($1.5 \times 10^6 \text{ N}\cdot\text{s}/\text{m}^3$), one can predict the bandwidth of this particular CMUT. The immersion bandwidth is limited by the antiresonance frequency, in which the average volume displacement of the circular membrane is equal to zero. Our simulation, based on the simple circular membrane approach, predicts the antiresonance frequency as 50 MHz. The plot in Fig. 2 suggests a 3-dB bandwidth between the frequencies 4 MHz and 36 MHz, which corresponds to a fractional 3-dB bandwidth of 160%.

B. Annular Array Design

The forward-viewing annular array is a complementary tool on a catheter probe used in intravascular imaging (Fig. 3). Because of the size limitations imposed by the guiding wire and the blood vessel structures, design and fabrication of the forward-viewing annular arrays present a major challenge. The annular array considered in this paper consists of 64 elements. The inner diameter of the array is 1.38 mm, and the outer diameter is 2.56 mm. This particular array configuration is larger than those commonly used in state-of-the-art intravascular imaging systems. It was designed and fabricated as a prototype and can be scaled down to meet the requirements of the intravascular imaging taking into consideration the reduction in the capacitance with the device area. Fig. 4 shows a micrograph of a fabricated, 64-element, forward-viewing annular array. For experimentation purposes, the bond pads, each with a size of $100 \times 100 \mu\text{m}^2$, are added to each element to allow wire bonding. The calculated capacitance of such a bond pad is approximately 0.615 pF, which is a large parasitic capacitance as compared to the calculated device capacitance of 0.826 pF. Normally, the array would be fabricated with an electrical through-wafer interconnect technique, which addresses each array element individually with a

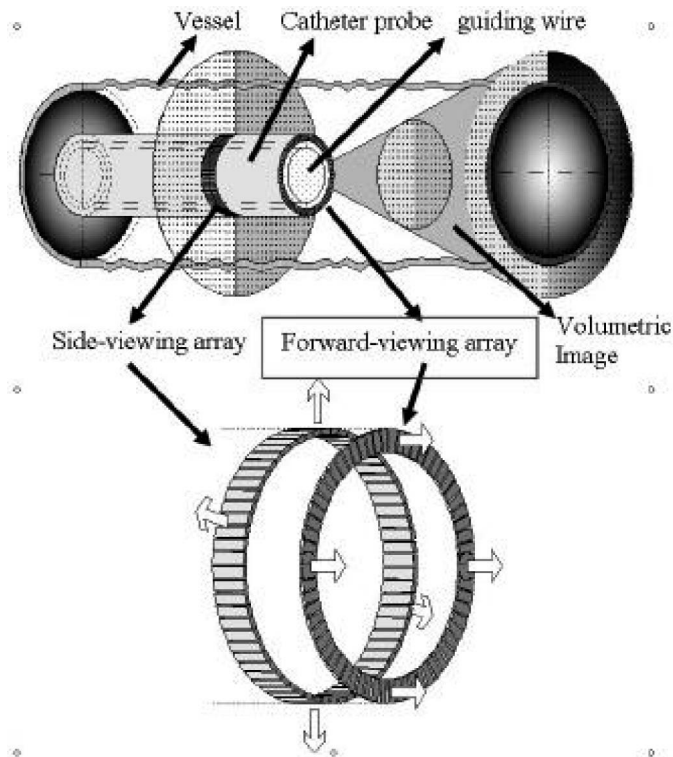


Fig. 3. Symbolic illustration of an intravascular catheter probe with a side-viewing and forward-viewing ring array in which the forward-viewing array acquires volumetric scans along the vessel.

low parasitic capacitance of 0.05 pF from the backside of the silicon wafer. This step is skipped for this prototype fabrication.

In general, CMUT elements are made of circular, hexagonal, or rectangular membranes. The size of the membrane determines the frequency response of the overall element. In the case of annular arrays, in which the elements are trapezoids, using such membranes results in inefficient use of area. However, for these kinds of arrays, maximizing the ratio of the membrane area (active area) to the total element area is critical in overall array performance. Increasing the active area increases the transduction efficiency and decreases the ratio of the parasitic capacitance to the active device capacitance. Therefore, the annular array element is designed as one trapezoidal membrane with posts as shown in Fig. 5, which also is called a tent membrane. The posts are needed to support the membrane so that it does not collapse under ambient pressure. In addition, the separation of the posts determines the frequency response of the element.

By using tent membranes, one can maximize the active area. The mechanical impedance of circular and rectangular membranes can be calculated by solving the differential equations that describe the equation of motion on the membrane [1]. Such a solution is not yet available for tent membranes. A 2-D numerical simulation using the finite-element method can be used to calculate the mechanical impedance of the tent membrane and predict the frequency response in immersion using equivalent circuit

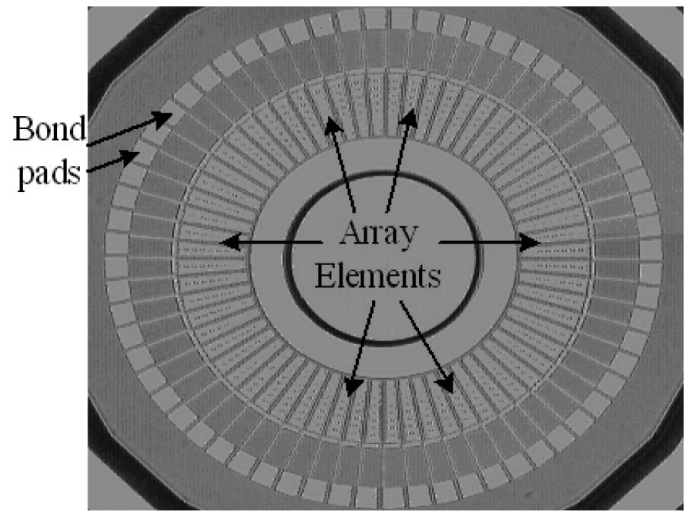


Fig. 4. Photograph of the forward-viewing annular array with 64 elements.

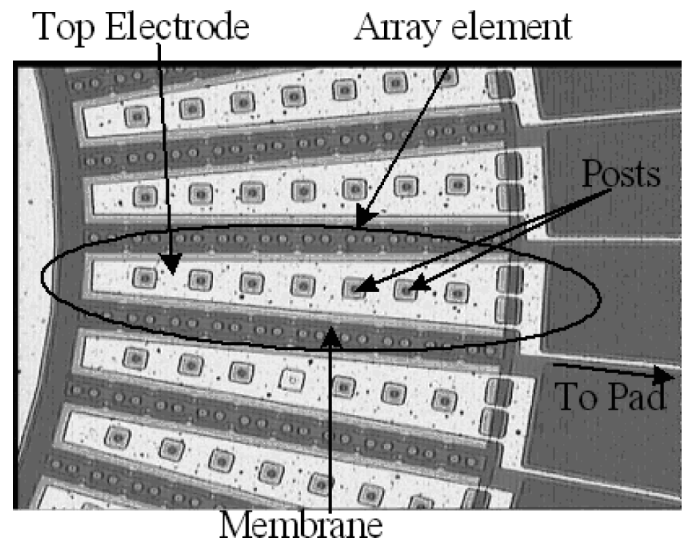


Fig. 5. A magnified picture of a portion of the forward-viewing annular array showing an array element.

modeling. In the equivalent circuit modeling, a simple but crude approximation uses the mechanical impedance of a circular membrane with a diameter equal to the separation between the posts. This is a first order approximation for immersion applications in which the acoustical impedance of the fluid dominates the mechanical response of the membrane. Fig. 2 shows the mechanical impedance of an array element calculated using such an approximation in which the posts are separated by $21 \mu\text{m}$.

C. Device Fabrication

The standard CMUT fabrication process starts with a low-resistivity silicon wafer. The silicon wafer is heavily doped to achieve good conductivity at the surface, which is the bottom plate (electrode) of the capacitor. Then, a

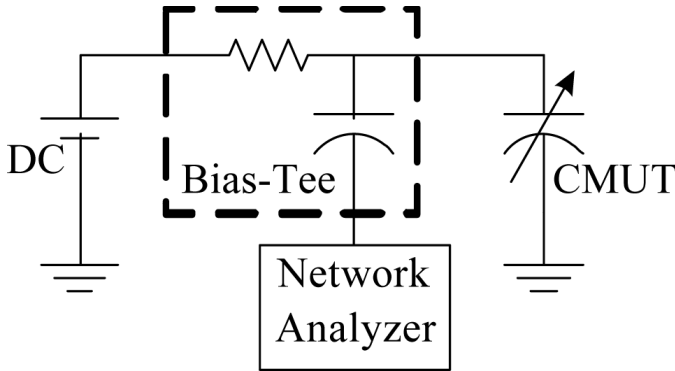


Fig. 6. Schematic of the experimental setup for input impedance measurements.

thin (1500 \AA) layer of low pressure chemical vapor deposition (LPCVD) Si_3N_4 (silicon nitride) is deposited as an etch stop for the sacrificial layer etching. Poly-crystalline silicon (polysilicon) is deposited and patterned in order to form the sacrificial layer that defines the membrane area. A second layer of LPCVD Si_3N_4 deposited on the sacrificial layer later forms the membrane. Several etch holes are dry etched into the Si_3N_4 membrane to allow a path for the potassium hydroxide (KOH) to selectively etch the sacrificial polysilicon layer. The first Si_3N_4 layer protects the silicon wafer from KOH during the sacrificial etch process. After the wet release of the membranes, the gap is sealed with a third layer of LPCVD Si_3N_4 deposition. The aluminum top electrode (the other plate of the capacitor) is sputtered on top of the membrane, which is later patterned. The top view of the device is shown in Fig. 5. Details of the CMUT fabrication process can be found in [5], [19]. The final gap and membrane thickness for this particular annular array are 0.12 \mu m and 0.88 \mu m , respectively.

III. EXPERIMENTAL RESULTS

The DC bias voltage that is required to operate CMUTs both in transmit and receive mode also determines the transduction efficiency. Therefore, the DC operating voltage is important. In the conventional mode of operation, it should not exceed the collapse voltage beyond which the restoring force of the mechanical spring, defined by the membrane, cannot balance the electrostatic attraction force. It should be close to the collapse voltage to ensure high-transduction efficiency [20]–[22]. The DC bias is applied to the CMUT through a bias-tee, which essentially adds DC and AC voltages as shown in the experimental setup (Fig. 6).

A. Electrical Input Impedance Measurements in Air

The electrical input impedance of a transducer is a first measure of its electrical and mechanical properties. It provides the resonant frequency of the transducer in air

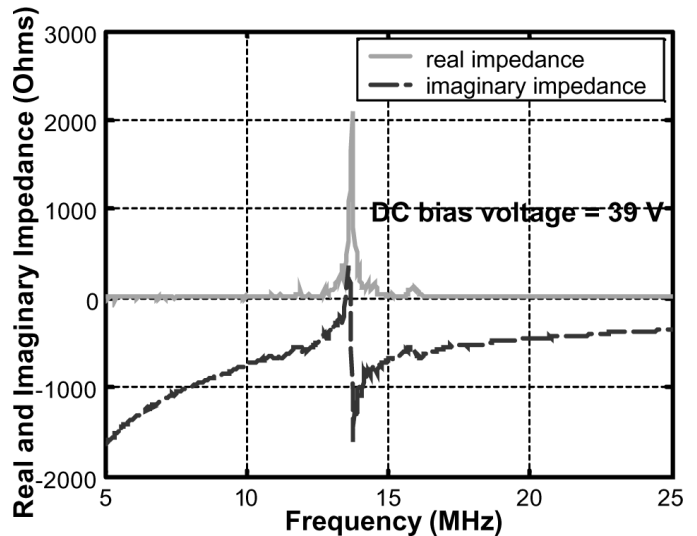
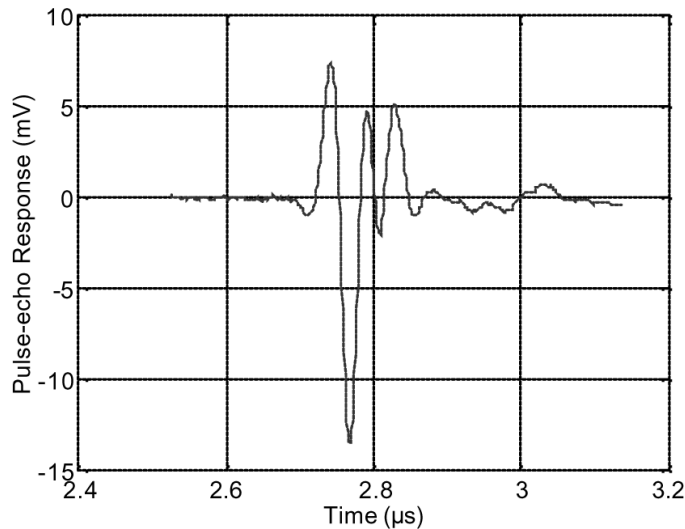


Fig. 7. The electrical input impedance of a single, annular-array element.

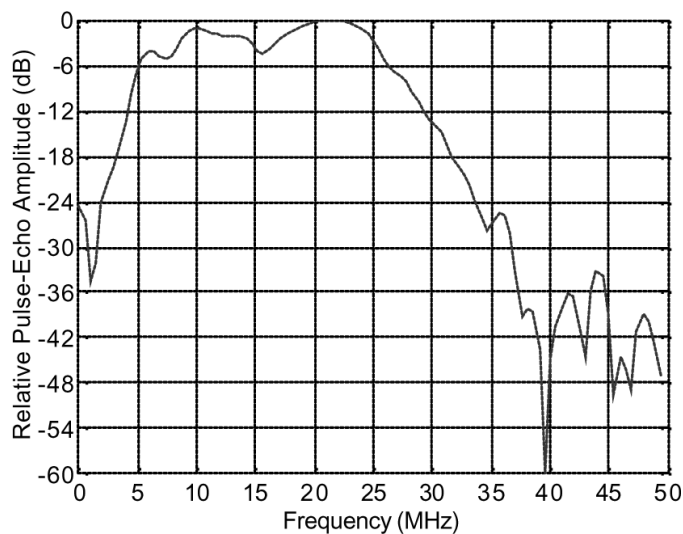
as well as its capacitance. These two data are the first check points between the measurements and predictions. The electrical input impedance measurements were carried out with a network analyzer (Model 8751A, Hewlett-Packard Co., Palo Alto, CA) using the experimental setup shown in Fig. 6. The network analyzer measures the input impedance of the device as a function of frequency. The data were captured and transferred to a computer display. The real and imaginary parts of the electrical input impedance of an array element are shown in Fig. 7. The resonant frequency of the array element was measured as 13.5 MHz in air. From the imaginary part of the measured impedance, we calculated the capacitance of each array element to vary between 2.5 pF and 3.1 pF throughout the array.

B. Pulse-Echo Measurements in Oil

We performed pulse-echo experiments in oil to measure the frequency response of the array elements. We preferred to use oil in pulse-echo measurements because oil provides electrical isolation for the electrical connections and mimics the tissue of vessel structure better than water regarding the acoustical properties such as speed and attenuation [7]. We connected six neighboring array elements together to reduce the effect of diffraction and to increase the SNR in the measurements. A steel block was placed 2 mm away as a plane reflector. The same experimental setup shown in Fig. 6 was used to perform the pulse-echo experiment by replacing the network analyzer with a pulser (Model 5055PR, Panametrics Inc., Waltham, MA). The echo signal received by the same transducer then was measured with an oscilloscope. The DC operating voltage was set to 45 V . The impulse response and its corresponding frequency spectrum (temporal frequency response) are shown in Fig. 8. The 6-dB frequency bandwidth is 21 MHz cen-



(a)



(b)

Fig. 8. (a) Time-domain, pulse-echo response, and (b) corresponding frequency spectrum for pulse excitation.

tered at 15.5 MHz that corresponds to 135% fractional bandwidth.

C. Absolute Pressure Measurements in Oil

For this experiment, the plane reflector was replaced with a calibrated needle hydrophone. The separation between the array and the hydrophone was 10 mm, which was measured by the time of flight of the pulse from the array to the hydrophone. The signal generator was set to supply 10 cycles of 5 MHz sinusoidal signal with 1 V amplitude, and the DC voltage was set to 40 V. The pulse received by the calibrated hydrophone was amplified and displayed on the oscilloscope. The measured signal amplitude at the hydrophone output was 0.8 mV. When compared to the calibration data of $0.5334 \mu\text{V}/\text{Pa}$ at 5 MHz, 0.8 mV corresponds to a pressure of 1.5 kPa/V at 5 MHz at a distance of 10 mm. This number was corrected for

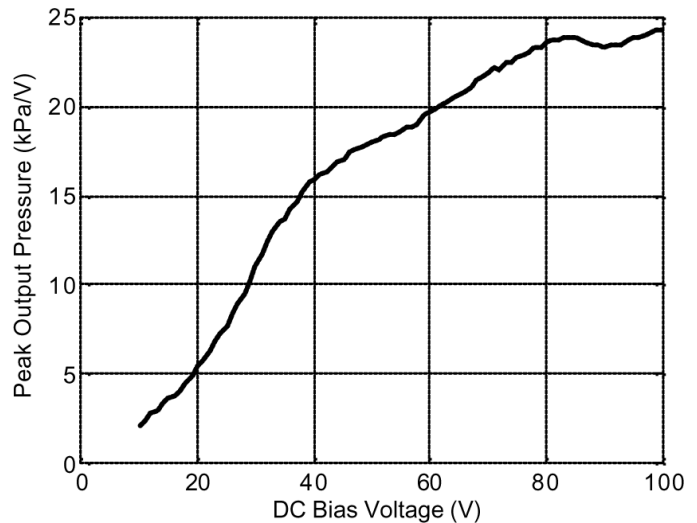


Fig. 9. Output pressure measured at 5 MHz by a calibrated hydrophone and corrected for diffraction loss and medium attenuation.

attenuation and diffraction to obtain the pressure at the surface of the annular array element. The attenuation loss is calculated from the attenuation coefficient of oil and the separation between the transducer and the hydrophone, which is 1.57 dB at 5 MHz. Calculating the diffraction loss is difficult because of the irregular transducer shape. However, a rectangular approximation is accurate enough at the far field of the transducer. Using this approximation, the diffraction loss was calculated as 18.9 dB, and the total loss added up to 20.5 dB. Correction of the calculated loss has resulted in an output pressure of 15.9 kPa/V for this particular array element. Fig. 9 shows the output pressure of the annular array elements as a function of the DC bias voltage. It is observed that the output pressure continues to increase with increasing DC bias voltage, although the membrane collapses at 40 V. This phenomenon is further discussed in Section IV.

The experiment was repeated at different frequencies with 40 V DC bias. The output pressure at the surface of the CMUT elements was measured as 16.1 kPa/V and 26.7 kPa/V at 10 MHz and 20 MHz, respectively.

D. Dynamic Range

The receive sensitivity of a transducer is traditionally known as the open-circuit receive sensitivity in which the output voltage is measured over an infinite impedance. Although this definition provides a means of comparison among transducers, it is not a true performance meter because it does not include the self-noise of the system. The SNR obtained at the output of the receiving amplifier per 1 Pa pressure is a better gauge of receive sensitivity and directly indicates the minimum signal we can detect above the noise level. It also includes the effect of the amplifier on the frequency response of the transducer. The output SNR is measured by using a piezoelectric transducer as a transmitter and the CMUT annular array element as

a receiver. The pressure generated by the transmitter is first measured with a calibrated hydrophone, then the hydrophone is replaced with the CMUT element. The custom receiving electronics was made of off-the-shelf components. The input stage was composed of two variable gain amplifiers (AD600, Analog Devices, Norwood, MA). The input impedance of AD600 is 100 Ohm. The input referred noise voltage is $1.4 \text{ nV}/\sqrt{\text{Hz}}$ and the input referred noise current is less than $0.1 \text{ pA}/\sqrt{\text{Hz}}$. We used two AD600 amplifiers in parallel to get an input impedance of 50 Ohm. Consequently, the input referred noise voltage is reduced to $1 \text{ nV}/\sqrt{\text{Hz}}$. Then, two of these stages are cascaded to get 60 dB gain, and a buffer amplifier (BUF04, Analog Devices, Norwood, MA) is added as the final stage to increase the current driving capability of the amplifier. Using this receiving electronics, we have obtained the output SNR of the annular array element as 44.1 dB/Pa at 10 MHz in 1-Hz bandwidth.

The dynamic range of an array element determines the final image quality (SNR of the image). Dynamic range is measured in a similar way to the two-way insertion loss, only it includes the self noise of the transducer and the receiving circuitry to the measurement. In a pitch-catch experiment, in which two identical transducers (one as a transmitter and one as a receiver) are placed facing each other, the two-way insertion loss is measured as the voltage across the receiving transducer normalized to the excitation voltage across the transmitting transducer. However, the dynamic range is measured as the SNR at the output of the receiving amplifier normalized to the excitation voltage across the transmitting transducer. Equivalently, one can use the output pressure value in transmit mode (Pa/V), and the output SNR in receive mode (dB/Pa in 1-Hz bandwidth) to calculate the dynamic range. Using the above values, we have calculated the dynamic range of the annular array element under test as 131.5 dB/V in 1-Hz bandwidth at 10 MHz.

IV. DISCUSSION

In our experiments, the input impedance of the array elements was measured where the main objective was to determine the resonant frequency in air and the capacitance of the device to make a comparison between measurements and predictions. Although we have not used an accurate calculation method to predict the resonant frequency of the device, the measured resonant frequency was consistent with the one predicted in Fig. 2. However, the measured capacitance was considerably larger than the expected device capacitance of 0.83 pF. The difference between the predicted value and the measured value was considered as the parasitic capacitance in which 0.62 pF of this was attributed to the pad and interconnection capacitances. The remaining 1 pF can be attributed to the connectors and the circuit board the array was mounted on.

Formally there are two basic ways to determine the frequency bandwidth of a CMUT device: complex analytical

calculations and finite element modeling (FEM) simulations. Each of these methods requires very extensive research for the tent structure and, therefore, will be considered in our future studies. Here, we predicted the resonance by a simple approach. We used a circular membrane approximation for the tent structure, in which the diameter of the circular membrane is equal to the postseparation of the tent membrane. In CMUTs, the first resonance frequency is damped with the large acoustic load in immersion applications, which gives the wide immersion bandwidth. Therefore, the prediction of the first resonance frequency is not very critical in determining the bandwidth. However, the antiresonance determines the upper cut-off frequency. Hence, calculating the antiresonance frequency is critical in predicting the bandwidth. Although our circular membrane assumption for predicting the upper cut-off frequency may result in error, our measurements show that we still can obtain the bandwidth without a considerable error through our simple calculation. Our future studies will focus on techniques such as finite element analysis for designing tent membranes operating at a given frequency with a desired fractional bandwidth.

We performed pulse-echo measurements in oil in which the purpose was to determine the frequency response of the array elements in immersion. In this experimental setup, rather than the conventional transmit/receive switching circuit, a simpler circuit was used as described in Section III. The echo signal was directly fed into the oscilloscope without any amplification. The result was a weak echo signal; however, it was not shaped with the receiving electronics. The Fourier transform of the echo signal reveals that the CMUT elements are indeed wideband with 6-dB (2-way) bandwidth extending from 5 to 26 MHz. This corresponds to a bandwidth of 21 MHz and a fractional bandwidth of 135%. This is somewhat less than that predicted by Fig. 2. We believe that the difference between predicted and measured bandwidth is due to the assumptions of the aforementioned model. The ripples in the frequency response at 8 and 16 MHz coincide with the thickness modes of a 500- μm thick silicon wafer. This is an indication of acoustical coupling into the silicon wafer via longitudinal waves. This kind of coupling can be avoided by incorporating an absorbing boundary on the back of the silicon wafer. The cross-talk between array elements, however, is expected to be less severe because of the geometry of annular elements. But this has not yet been investigated.

The pressure output of the array elements was measured with a calibrated hydrophone. The results show that these particular elements have high output pressure capability. The linearity of the output also was tested, and it was found that the output pressure increased linearly with respect to the amplitude of the AC input signal that was swept from 1 V to 16 V. The DC bias voltage also was swept from 10 V to 100 V to verify its effect on the CMUT operation. Normally, the output pressure of the CMUT should increase linearly up to the collapse voltage. Beyond the collapse voltage, the membrane should col-

lapse on to the substrate and cease operating. The linear behavior of the CMUT with respect to the bias voltage is observed in Fig. 9 up to the collapse voltage of 40 V. What happens beyond collapse cannot be explained with the simple modeling used here. Finite-element simulations show that, although the membrane collapses on to the substrate for DC bias voltages above the collapse voltage, only the center portion of the membrane touches the bottom, leaving a ring of membrane area still vibrating. Recently it was shown that it is possible to get high transduction efficiency from CMUTs operated in this mode, as predicted in [23] and [24]. This effect is demonstrated in Fig. 9.

The dynamic range of the annular array element was measured to be 131.5 dB/V/Hz. This means, for example, a dynamic range of 155 dB with 15 V excitation. Considering the diffraction and attenuation in human body, 155 dB dynamic range corresponds to a pulse-echo range of approximately 20 mm at 25 MHz, in which a 120-dB loss is due to medium attenuation and a 35-dB loss is due to diffraction. That is, a single annular array element, excited with 15 V at 25 MHz, can pick up reflections from a target at 20 mm with 0 dB SNR. At lower frequencies the imaging depth increases considerably because of the decrease in the attenuation losses, 30 mm at 20 MHz and 90 mm at 10 MHz. The overall SNR of an array imaging system is directly proportional to single-element's SNR, the number of transmit elements and square root of the number of receive elements ($SNR = SNR_0 \times N_t \times \sqrt{N_r}$). Regarding the constraints imposed by the system complexity issues, synthetic aperture and synthetic phased-array techniques are suitable for imaging applications with forward-viewing annular arrays [14], [25]–[27]. Assuming an image reconstruction based on synthetic aperture with a single, active element at each firing, the overall SNR becomes directly proportional to the single-element's SNR and square root of the element count (i.e., $N_t = 1$, $N_r = N$ and thus $SNR = SNR_0 \times \sqrt{N}$). Alternatively, if the image reconstruction is based on synthetic, phased-array processing, then considering only the nonredundant transmit-receive element combinations, the SNR becomes proportional to $SNR_0 \times N/\sqrt{2}$. In conclusion, the annular array reported in this paper can view 20 mm depth at 25 MHz with 18 dB and 33 dB image SNR for synthetic aperture and synthetic phased array, respectively.

The trade-off between element sensitivity and directivity is critical in forward-viewing annular array design. The element size must be small enough to insonify the whole image field, and the transmit and receive capability of the element is limited by its size. However, the lateral inter-element distance is strictly constrained by spatial Nyquist sampling criteria, and the radial extension is constrained by the view angle requirement. To obtain high-element sensitivity while meeting the lateral sampling requirement, we used a large radial extent for our initial experimental tests in which the aim was to demonstrate the first annular CMUT array based on the tent structure. Our current studies involve design and testing of annular arrays with equal element size in lateral and radial extensions.

We also address that the device fabricated and presented in this paper has LPCVD Si_xN_y membranes. Although it is not a part of the CMOS process and not suitable for postprocessing CMOS chips, LPCVD is considered as a standard micromachining process. The CMUT process used for fabrication of the CMUT array possesses all the advantages of the integrated circuits (IC) technology, such as ease of fabrication, batch production, and repeatability. For the CMUT array technology considered here, the receive electronics and the CMUTs should be fabricated separately and integrated with through-wafer electrical interconnects and flip-chip bonding technology [9].

V. CONCLUSIONS

In this paper, we presented the design and fabrication of the first 64-element, forward-viewing annular CMUT arrays and showed the experimental characterization results. The results demonstrate that CMUT annular array elements indeed have wide frequency bandwidth and a high dynamic range. Considering these two key features together with potentials due to CMUT fabrication based on silicon processing, we conclude that forward-viewing annular CMUT arrays are good candidates for medical imaging applications, especially in invasive ultrasound in which the probe size, efficiency of small-sized elements, and electronic integration have critical importance.

REFERENCES

- [1] M. I. Haller and B. T. Khuri-Yakub, "A surface micromachined electrostatic ultrasonic air transducer," *IEEE Trans. Ultrason., Ferroelect., Freq. Contr.*, vol. 43, pp. 1–6, Jan. 1996.
- [2] D. W. Schindel, D. A. Hutchins, L. Zhou, and M. Sayer, "The design and characterization of micromachined air coupled capacitance transducers," *IEEE Trans. Ultrason., Ferroelect., Freq. Contr.*, vol. 42, pp. 42–50, May 1995.
- [3] H. T. Soh, I. Ladabaum, A. Atalar, C. F. Quate, and B. T. Khuri-Yakub, "Silicon micromachined ultrasonic immersion transducers," *Appl. Phys. Lett.*, vol. 69, pp. 3674–3676, Dec. 1996.
- [4] A. G. Bashford, D. W. Schindel, and D. A. Hutchins, "Micromachined ultrasonic capacitance transducers for immersion applications," *IEEE Trans. Ultrason., Ferroelect., Freq. Contr.*, vol. 45, pp. 367–375, Mar. 1998.
- [5] X. C. Jin, I. Ladabaum, L. Degertekin, S. Calmes, and B. T. Khuri-Yakub, "Fabrication and characterization of surface micromachined capacitive ultrasonic transducers," *IEEE J. Microelectromech. Syst.*, vol. 8, pp. 100–114, Mar. 1999.
- [6] X. C. Jin, Ö. Oralkan, F. L. Degertekin, and B. T. Khuri-Yakub, "Characterization of one-dimensional capacitive micromachined ultrasonic immersion transducer arrays," *IEEE Trans. Ultrason., Ferroelect., Freq. Contr.*, vol. 48, pp. 750–760, May 2001.
- [7] Ö. Oralkan, A. S. Ergun, J. A. Johnson, M. Karaman, U. Demirci, K. Kaviani, T. Lee, and B. T. Khuri-Yakub, "Capacitive micromachined ultrasonic transducers: Next generation arrays for acoustic imaging?," *IEEE Trans. Ultrason., Ferroelect., Freq. Contr.*, vol. 49, pp. 1596–1610, Nov. 2002.
- [8] Ö. Oralkan, A. S. Ergun, C.-H. Cheng, J. A. Johnson, M. Karaman, T. H. Lee, and B. T. Khuri-Yakub, "Volumetric imaging using 2D capacitive micromachined ultrasonic transducer arrays (CMUTs): Initial results," in *IEEE Ultrason. Symp., Munich, Germany*, 2002, pp. 1083–1086.
- [9] Ö. Oralkan, A. S. Ergun, C.-H. Cheng, J. A. Johnson, M. Karaman, T. H. Lee, and B. T. Khuri-Yakub, "Volumetric imag-

ing using two-dimensional capacitive micromachined ultrasonic transducer arrays," *IEEE Trans. Ultrason., Ferroelect., Freq. Contr.*, to be published.

- [10] M. O'Donnell, M. J. Eberle, D. N. Stephens, J. L. Litzza, B. M. Shapo, J. R. Crowe, C. D. Choi, J. J. Chen, D. M. W. Muller, J. A. Kovach, R. L. Lederman, R. C. Ziegenbein, C. C. Wu, K. San Vicente, and D. Bleam, "Catheter arrays: Can intravascular ultrasound make a difference in managing coronary artery disease," in *Proc. IEEE Ultrason. Symp.*, 1997, pp. 1447–1456.
- [11] F. W. van der Steen, E. I. Cespedes, C. L. de Korte, S. G. Carlier, W. Li, F. Mastik, C. T. Lancee, J. Borsboom, F. Lupotti, R. Krams, P. W. Serruys, and N. Bom, "Novel developments in intravascular imaging," in *Proc. IEEE Ultrason. Symp.*, 1998, pp. 1733–1742.
- [12] J. Schulze-Clewing, M. J. Eberle, and D. N. Stephens, "Miniaturized circular array," in *Proc. IEEE Ultrason. Symp.*, 2000, pp. 1253–1254.
- [13] J. R. Crowe, B. M. Shapo, D. N. Stephens, D. Bleam, M. J. Eberle, E. I. Cespedes, C. C. Wu, D. W. M. Muller, J. A. Kovach, R. J. Lederman, and M. O'Donnell, "Blood speed imaging with an intraluminal array," *IEEE Trans. Ultrason., Ferroelect., Freq. Contr.*, vol. 47, pp. 672–681, May 2000.
- [14] Y. Wang, D. N. Stephens, and M. O'Donnell, "Optimizing the beam pattern of a forward-viewing ringannular ultrasound array for intravascular imaging," *IEEE Trans. Ultrason., Ferroelect., Freq. Contr.*, vol. 49, pp. 1652–1664, Dec. 2002.
- [15] Ö. Oralkan, X. C. Jin, F. L. Degertekin, and B. T. Khuri-Yakub, "Simulation and experimental characterization of a 2-D capacitive micromachined ultrasonic transducer array element," *IEEE Trans. Ultrason., Ferroelect., Freq. Contr.*, vol. 46, pp. 1337–1340, Nov. 1999.
- [16] C. H. Cheng, A. S. Ergun, and B. T. Khuri-Yakub, "Electrical through wafer interconnects with 0.05 pico farads parasitic capacitance on 400 μm thick silicon substrate," in *Solid State Sensor, Actuator and Microsystems Workshop, Hilton Head Island, SC*, pp. 157–160, June 2002.
- [17] I. Ladabaum, X. C. Jin, H. T. Soh, A. Atalar, and B. T. Khuri-Yakub, "Surface micromachined capacitive ultrasonic transducers," *IEEE Trans. Ultrason., Ferroelect., Freq. Contr.*, vol. 45, pp. 678–690, May 1998.
- [18] W. P. Mason, *Electromechanical Transducers and Wave Filters*. London: Van Nostrand, 1948.
- [19] X. C. Jin, I. Ladabaum, and B. T. Khuri-Yakub, "The microfabrication of capacitive ultrasonic transducers," *IEEE J. Microelectromech. Syst.*, vol. 7, pp. 295–302, Sep. 1998.
- [20] F. V. Hunt, *Electroacoustics: The Analysis of Transduction, and Its Historical Background*. Cambridge: Harvard Univ. Press, 1954.
- [21] W. Kuhl, G. R. Schodder, and F. K. Schodder, "Condenser transmitters and microphones with solid dielectric for airborne ultrasonics," *Acustica*, vol. 4, pp. 520–525, 1954.
- [22] J. Fraser and P. Reynolds, "Finite-element method for determination of electromechanical coupling coefficient for piezoelectric and capacitive micromachined ultrasonic transducers," presented at the 140th Joint Meeting of ASA/NOISE-CON, 2000.
- [23] B. Bayram, E. Hæggström, G. G. Yaralioglu, and B. T. Khuri-Yakub, "A new regime for operating capacitive micromachined ultrasonic transducers," *IEEE Trans. Ultrason., Ferroelect., Freq. Contr.*, vol. 50, pp. 1184–1190, Sep. 2003.
- [24] Y. Huang, B. Bayram, A. S. Ergun, E. Hæggström, C. H. Cheng, and B. T. Khuri-Yakub, "Collapsed region operation of capacitive micromachined ultrasonic transducers based on wafer-bonding technique," presented at *Proc. IEEE Ultrason. Symp.*, Honolulu, HI, 2003, pp. 1161–1164.
- [25] M. Karaman, P.-C. Li, and M. O'Donnell, "Synthetic aperture imaging for small scale systems," *IEEE Trans. Ultrason., Ferroelect., Freq. Contr.*, vol. 42, pp. 429–442, May 1995.
- [26] M. Karaman and M. O'Donnell, "Subaperture processing for ultrasonic imaging," *IEEE Trans. Ultrason., Ferroelect., Freq. Contr.*, vol. 45, pp. 126–135, Jan. 1998.
- [27] J. A. Johnson, M. Karaman, and P. T. Khuri-Yakub, "Synthetic phased array image formation and restoration," in *Proc. IEEE Int. Conf. Acoust. Speech Signal Process.*, May 13–17, 2002, pp. 2885–2888.



Utkan Demirci (S'01) received his B.S. degree in Electrical Engineering in 1999 as a James B. Angell Scholar with Summa Cum Laude from University of Michigan, Ann Arbor. He received his M.S. degree from Stanford University in 2001, and working towards doctor of philosophy degree in Electrical Engineering. He is one of the few recipients of the Full Presidential Scholarship given by the Turkish Ministry of Education. He is a corecipient of the 2002 Outstanding Paper Award of the IEEE Ultrasonics, Ferroelectrics and Frequency Control Society. He is the winner of Stanford University BASES Entrepreneur's Challenge Competition in 2004. He is a member of Phi Kappa Phi, National Honor Society. He is a member of the IEEE.

His research interests involve MEMS, especially, micromachined ultrasonic microfluid droplet ejector arrays for high resolution printing and biological applications, capacitive micromachined ultrasonic arrays (CMUTS) for medical imaging applications, and 2D acoustic ordered crystals.



A. Sanli Ergun (S'96–A'98) was born in Ankara, Turkey in 1969. He received his B.S., M.S. and Ph.D. in 1991, 1994, and 1999, respectively, all in Electrical and Electronics Engineering from Bilkent University, Ankara, Turkey.

He is now in the E. L. Ginzton Laboratory, Stanford University as an engineering research associate. His main research interests are acoustics, ultrasound, microelectromechanical systems (MEMS), and microwave electronics.



Ömer Oralkan (S'93) was born in İzmit, Turkey, in 1973. He received the B.S. degree from Bilkent University, Ankara, Turkey, in 1995, and the M.S. degree from Clemson University, Clemson, SC, in 1997, both in electrical engineering. He is currently pursuing a Ph.D. degree in electrical engineering at Stanford University, Stanford, CA.

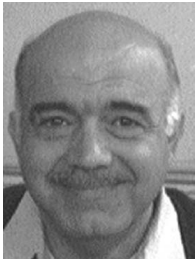
From 1995 to 1996, he was a hardware and network engineer at Bilkent University Computer Center, Ankara, Turkey. In the summer of 1997, he worked as a process engineer at the National Semiconductor Research Laboratories, Santa Clara, CA. His past and present research interests include analog and digital circuit design, micromachined sensors and actuators, and semiconductor device physics and fabrication. His current research focuses on front-end electronic circuit design for 2-D capacitive micromachined ultrasonic transducer arrays for hand-held 3-D ultrasonic imaging systems. He is a corecipient of the Best Paper award presented at the IEEE International Symposium on the Physical and Failure Analysis (IPFA). He is a member of IEEE.



Mustafa Karaman (S'88–S'89–M'89–M'93–M'97) received the B.Sc. degree from the Middle East Technical University, Ankara, Turkey and the M.Sc. and Ph.D. degrees from Bilkent University, Ankara, Turkey in 1986, 1988, and 1992, respectively, all in electrical and electronics engineering. From 1993 to 1994, he was a post-doctoral fellow in the Biomedical Ultrasonics Laboratory in the Bioengineering Department, University of Michigan, Ann Harbor.

From 1995 to 1996, he was on the faculty with the Electrical and Electronics Engineering Department of Kırıkkale University, Kırıkkale, Turkey, first as Assistant Professor and later as Associate Professor. In 1996, he joined Başkent University, Ankara, Turkey, as the Chairman of Electrical and Electronics Engineering and Acting Chairman of the Computer Engineering Department and served in founding these departments. He was a visiting scholar in the Biomedical Ultrasonics Laboratory at the University of Michigan, Ann Arbor, and in the E. L. Ginzton Laboratory at Stanford University, Stanford, CA, in the summer terms of 1996–1997 and 1999, respectively. In 2000, he joined the E.L. Ginzton Laboratory at Stanford University, Stanford, CA, as a visiting faculty in electrical engineering, where he is currently working on signal processing and system design for ultrasonic imaging using capacitive micromachined ultrasonic transducer arrays.

In 1996, Dr. Karaman was awarded H. Tugac Foundation Award of Turkish Scientific and Technical Research Council for his contributions to ultrasonic imaging. Dr. Karaman is a member of the IEEE.



Butrus T. Khuri-Yakub (S'70–S'73–M'76–SM'87–F'95) was born in Beirut, Lebanon. He received the B.S. degree in 1970 from the American University of Beirut, the M.S. degree in 1972 from Dartmouth College, and the Ph.D. degree in 1975 from Stanford University, Stanford, CA, all in electrical engineering.

He joined the research staff at the E. L. Ginzton Laboratory, Stanford University in 1976 as a Research Associate. He was pro-

moted to a Senior Research Associate in 1978 and to a Professor of Electrical Engineering (Research) in 1982. He has served on many university committees in the School of Engineering and the Department of Electrical Engineering. Presently, he is the Deputy Director of the E. L. Ginzton Laboratory.

He has been teaching both at the graduate and undergraduate levels for over 15 years, and his current research interests include in situ acoustic sensors (temperature, film thickness, resist cure, etc.) for monitoring and control of integrated circuits manufacturing processes, micromachining silicon to make acoustic materials and devices such as airborne and water immersion ultrasonic transducers and arrays, fluid ejectors, and ultrasonic nondestructive evaluation and acoustic imaging and microscopy.

He has authored over 300 publications and has been principal inventor or co-inventor of 54 issued patents. Dr. Khuri-Yakub is a Senior Member of the Acoustical Society of America, and a Member of Tau Beta Pi. He is an Associate Editor of *Research in Nondestructive Evaluation*, a journal of the American Society for Nondestructive Testing. He received the Stanford University School of Engineering Distinguished Advisor Award, June 1987, and the Medal of the City of Bordeaux for contributions to NDE, 1983.